Received: 30 October 2017 | Revised: 1 February 2018 | Accepted: 2 February 2018

DOI: 10.1002/gj.3187

WILEY

SPECIAL ISSUE ARTICLE

Genetic implications for the Damajianshan W-Cu-As polymetallic deposit in Lvchun, Southwest China: Constraints from H–O, He–Ar, S, and Pb isotopes

Lei Zhang[1] | Guishan Zhang[1] | Hanjie Wen[2,3] | Chaojian Qin[2,3] | Rongxi Li[1] | Chuanwei Zhu[2,3] | Shengjiang Du[4]

[1] School of Earth Science and Resources, Chang'an University, Xi'an, China

[2] State Key Laboratory of Ore Deposit Geochemistry, Chinese Academy of Sciences, Guiyang, China

[3] University of Chinese Academy of Sciences, Beijing, China

[4] Guizhou Geological Survey, Guiyang, China

Correspondence
Guishan Zhang, School of Earth Science and Resources, Chang'an University, Xi'an 710054, China.
Email: zygszh@chd.edu.cn

Funding information
National Key R&D Program of China, Grant/Award Number: 2017YFC0602503; the strategic Priority Research Program (B) of Chinese Academy of Sciences, Grant/Award Number: XDB18030302; 973 Program, Grant/Award Number: 2014CB440904; Guizhou Scientific and Technological Innovation Team, Grant/Award Number: 2017-5657; Fundamental Research Foundation of the Central Universities, Grant/Award Numbers: 300102278111 and 310827172003

Handling Editor: G. Yang

The Sanjiang Tethyan domain in SE Asia is one of the most important mineral belts in China. The Damajianshan (DMJS) W-Cu-As polymetallic deposit is located in the southern part of Sanjiang Tethyan domain, related to Triassic quartz porphyry. Detailed exploration thereafter shows that the reserves of W, Cu, and As are 0.09, 0.42, and 0.12 Mt, respectively. The W is a typical oxyphile element and always coexisted with Sn–Li–Be–Nb–Ta. The Cu–As are typical sulphophile elements and always coexisted with Au–Ag–Pb–Zn–Sb–Hg. It is rarely reported that a deposit preserves tungsten and copper–arsenic simultaneously in the southern Sanjiang region. In this study, the S–Pb isotopic ratios of sulphides, the H–O isotopic compositions of fluid inclusions in hydrothermal quartz, and the He–Ar isotopic ratios of fluid inclusions in sulphides were analysed to constrain the origin of the DMJS deposit. Studies have shown that the $\delta^{34}S$ values of sulphides from ores are mainly between −6.17‰ and +0.02‰; the sulphur isotope compositions indicate that the ore-forming materials might originate from deep sources. The Pb isotope characteristics indicate that the ore metals might originate from deep sources and be closely related to the quartz porphyry. The $\delta^{18}O_{fluid}$ values of ore-forming fluids calculated from hydrothermal quartz range from −5.5‰ to +7.5‰, and the δD values of the fluid inclusions in quartz are from −81.7‰ to −50.2‰. The H–O isotope systematics indicate that the ore fluids in the DMJS deposit were probably initially sourced from magmatic water and later gradually mixed with Mesozoic meteoric water. Fluid inclusions in pyrite, chalcopyrite, arsenopyrite, and pyrrhotite possess $^{3}He/^{4}He$ ratios of 0.02–0.05 Ra, and their $^{40}Ar/^{36}Ar$ ratios range from 562.47 to 4159.15, indicating a complete crustal fluids and with higher radiogenic ^{40}Ar. The noble gas isotopic data, along with the stable isotopic data, suggest that the ore-forming fluids have a deep source. The unique geologic structure of the Sanjiang Tethys tectonic metallogenic region and the evolution of ore-forming fluids both promoted the formation of this rare DMJS deposit.

KEYWORDS

noble gas isotope, Sanjiang Tethys, stable isotope, W-Cu-As polymetallic deposit

1 | INTRODUCTION

The Tethys is a global latitudinal tectonic belt in the southern margin of Eurasia continent, located between Eastern European platform, Kazakhstan block, Tarim, North China, Yangtze, Indo-China, Arabian cratons, Indian Plate, and African Plate and composed of terrains of Anatolides, Transcaucasia, Alborz, Lut, Central Iran, Afghanistan, Pamirs, Northern Qiangtang, Southern Qiangtang, Lhasa, Baoshan, Sibu-masu, and Western Myanmar as well as the orogenic belts among these blocks. It was formed by two-stage subduction and collision between these blocks which commenced in Late Palaeozoic and continued to Cenozoic, called Paleo-Tethyan and Neo-Tethyan tectonic events.

The Sanjiang Tethyan domain is one of the most important mineralization belts in China. A large number of studies have shown that the Sanjiang Tethyan domain has experienced a superposed transition from the Tethys tectonic evolution in Late Palaeozoic to the continental collision orogeny in Cenozoic, associated with a great mass of

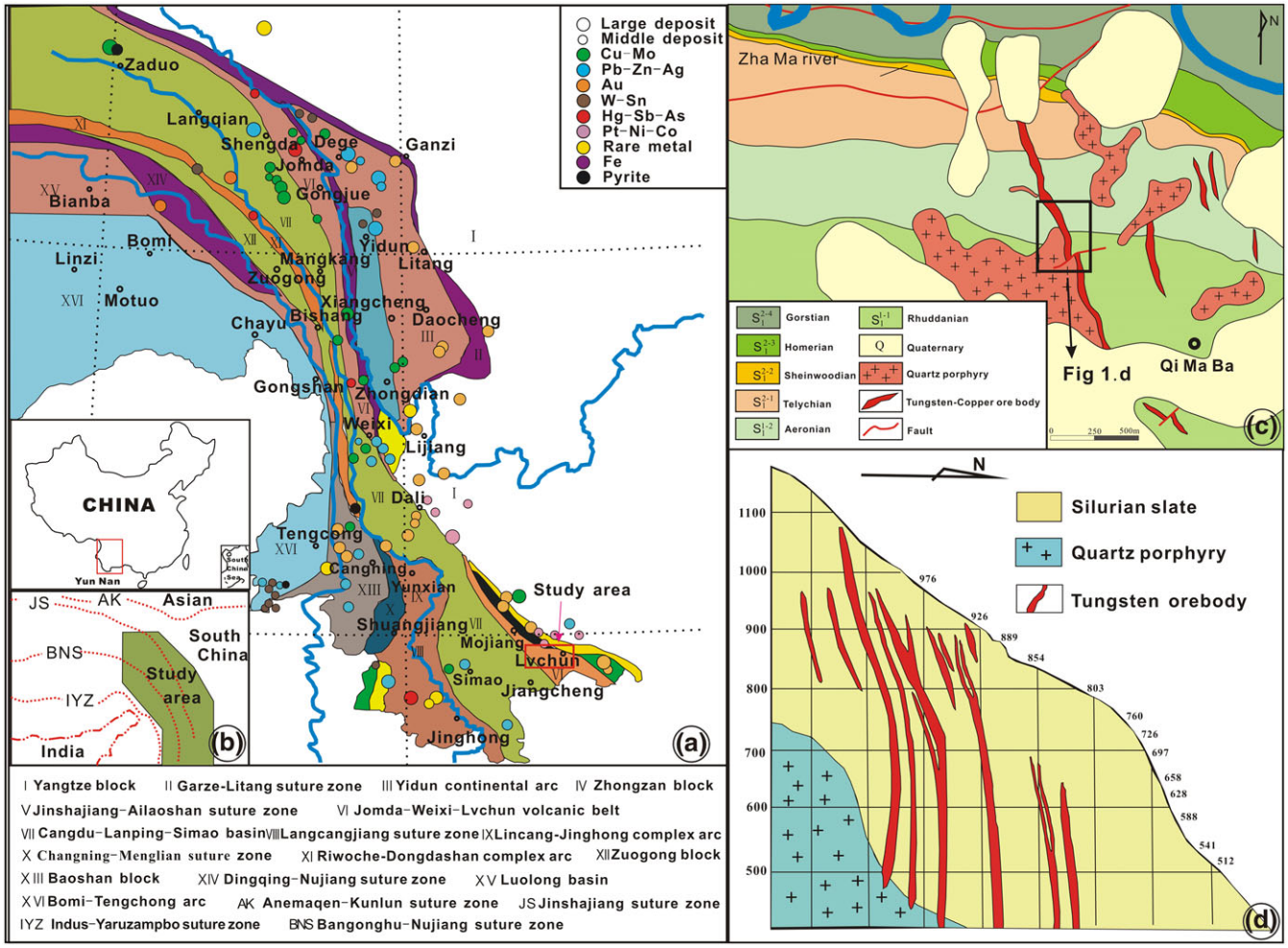

FIGURE 1 Geological map of the study area. (a, b) Geological map showing tectonic framework and distribution of ore deposits in the Sanjiang Tethys (modified after Deng et al., 2010; Deng et al., 2011; Deng, Wang, Li, & Wang, 2014; Hou, Pan, et al., 2007a; Hou, Zaw, et al., 2007b; Hou, Pan, et al., 2007a; Liu, Li, & Ye, 1993); (c, d) regional geological and profile map of the Damajianshan deposit (modified after Zhang et al., 2015) [Colour figure can be viewed at wileyonlinelibrary.com]

multistage mineralization and the formation of large volumes of metallic mineral deposits (Deng, Wang, & Li, 2012; Deng, Yang, & Wang, 2011; Li, Liu, & Wei, 1993; Pan et al., 2004; Wang, Deng, Zhang, Xue et al., 2010a; Wang, Deng, Zhang, & Yang, 2010b). Various deposit types in the Sanjiang Tethyan domain occur in different metallogenic epochs and display a trend from simple to complex natures corresponding to the tectonic evolution of the Sanjiang Tethys from Early Palaeozoic to Tertiary. In the Early Palaeozoic metallogenic epoch, mineralizations took place only along the boundaries of scattered blocks resulted from the break-off of the continental block, and only minor hydrothermal Pb–Zn deposits were formed. In the Late Palaeozoic metallogenic epoch, mineralizations mainly occurred in arc-basin systems, resulting in the formation of a number of valcanic hosted massive sulfide (VHMS) deposit with Cu–Zn, Cu–Pb–Zn, and Fe–Cu associations. In the Late Triassic, at least three types of ore deposits occurred in the postcollisional crustal extension settings caused by the lithospheric delamination or slab break-off and the arc-basin systems (Hou, Pan, Yang, & Qu, 2007a). The VHMS deposits occur in both postcollisional extensional basins and intra-arc rift basins, whereas the porphyry Cu deposits and/or skarn-type polymetallic deposits were formed in arc volcano-magmatic complexes and the epithermal Ag–Au–Hg deposits in the back-arc felsic volcanic rocks. Cu, Pb–Zn, Ag, Au, and Sn are the most important resources in this domain (Wang, Deng, Carranza, & Santosh, 2014). In contrast, only a few tungsten mineralizations were reported in the Sanjiang Tethyan domain. There are some small-scale tungsten deposits in the central and northern Sanjiang Region, such as the Lushui, Shangli-La, Jiangda, and Yulong deposits (Deng et al., 2012; Deng, Wang, Li, Li, & Wang, 2013; Hou et al., 2003; Hou, Pan, et al., 2007a; Hu et al., 2004; Li & Li, 2007; Qiu, Dai, & Pu, 1994; Sun et al., 2009; Xue et al., 2007; Zaw, Peters, Cromie, Burrett, & Hou, 2007). In this paper, we describe some basic geological and geochemical features of the DMJS deposit. Data on He–Ar–H–O–S–Pb isotope are used to analyse the formation mechanism and the origin of the deposit. The deposit formed in the same period of the same mineral belt generally have similar geological background and metallogenic essential factors. There are 23 Indosinian granitic rock mass in this area. So the study on the DMJS ore deposit as a typical one will help to understand the evolution and mineralization mechanism of ore-forming fluids in the same period and in the same region. Understanding its metallogensis has important strategic significance and industrial value and was a boon for this region.

2 | GEOLOGICAL SETTING

The DMJS deposit is located in Lvchun County, Yunnan Province, SW China. Tectonically, the deposit is in the southernmost part of the Jomda–Weixi–Lvchun arc-volcanic belt, which was formed at the end of the late Palaeozoic to early Mesozoic (Deng et al., 2010; Deng et al., 2012; Hou, Pan, et al., 2007a; Hou, Zaw et al., 2007b; Li, Liu, & Wang, 1999; Pan, Chen, & Li, 1997; Yin, Pan, Wang, Li, & Wang, 2006; Figure 1a,b). The DMJS deposit was first discovered during a 1:200,000 regional geological survey by the Geological Survey Team of Yunnan province in 1970s and identified as a Cu–As deposit. In recent years, the further exploration have confirmed that it was the quartz-vein-type W–Cu–As polymetallic deposit related to Triassic quartz porphyry (Figure 1).

The DMJS deposit has 0.09 Mt metal reserves of W with an average grade of 0.35 wt.%, ranging from 0.15 wt.% to 1.2 wt.% WO_3, which belongs to large scale W deposit (≥0.05 Mt) according to the industrial classification of ore deposits in China. Subsequent detailed exploration showed that the metal reserves of Cu and As are 0.42 Mt (ore grade from 0.37 wt.% to 3.18 wt.%) and 0.12 Mt (ore grade from 2.73 wt.% to 27.70 wt.%), respectively, corresponding to medium scale for Cu (0.1–0.5 Mt) and large scale for As (≥0.05 Mt). Besides W, Cu, and As, the associated metals resources of Pb–Zn, Bi, and Mo also attain industrial value.

To date, 10 W-bearing orebodies have been discovered (Figure 1 d). These orebodies commonly extend about 60–430 m in vertical direction with 3.5–18 m thickness. Magmatic activity in the deposit is marked by the intrusion of Triassic quartz porphyry and some lamprophyres. Spatial-temporally, the intrusion of Triassic quartz porphyry is closely connected to the formation of the DMJS hydrothermal tungsten polymetallic deposit. The W-bearing orebodies are mainly distributed within the external contact zone of the quartz porphyry. The wall rock is a set of Silurian slate (Figure 1c,d). A great variety of metasomatic alterations can be found in the deposit, including potassic alteration, silicification, sericitization, pyritization, epidotization, and tourmalinization. Faults are the dominant structural features in the study area, and they provided favourable metallogenic and ore-hosting space for the movement and deposition of ore-forming fluid.

The ore mineralogy in DMJS deposit is complex. The main ore minerals are arsenopyrite, pyrite, chalcopyrite, scheelite, wolframite, galena, sphalerite, and several Pb–Bi–sulphosalt and Pb–Sb–sulphosalt (Figure 2). The gangue minerals are quartz, dolomite, manganocalcite, and others. It is very common for these minerals to occur as mutual metasomatic inclusions and interpenetrations. According to the mineral intercalating relationships, the mineral formation sequence had four stages (Zhang et al., 2015). From the earliest to latest, the four stages can be classified as silicate, quartz–sulphide, sulphide–oxide, and carbonate. The deposit includes two main ore types, massive ores and vein ores. The massive ores are a medium grained arsenopyrite–chalcopyrite ores usually with small amounts of pyrrhotite and pyrite. Galena, sphalerite, and several sulphosalts occur in minor amounts. The vein ores are scheelite and wolframite usually with small amounts of molybdenite and manganocalcite.

The mineralization of tungsten are complex and can be approximately divided into three types: (a) single type—there is only tungsten mineralization except for that with local molybdenum mineralization and no other industrial mineralization. Alterations are single and mainly silication, associated with sericitization, always appearing on the upper middle of mining, such as middle of levels 926, 889, 854, and 803; (b) mixed

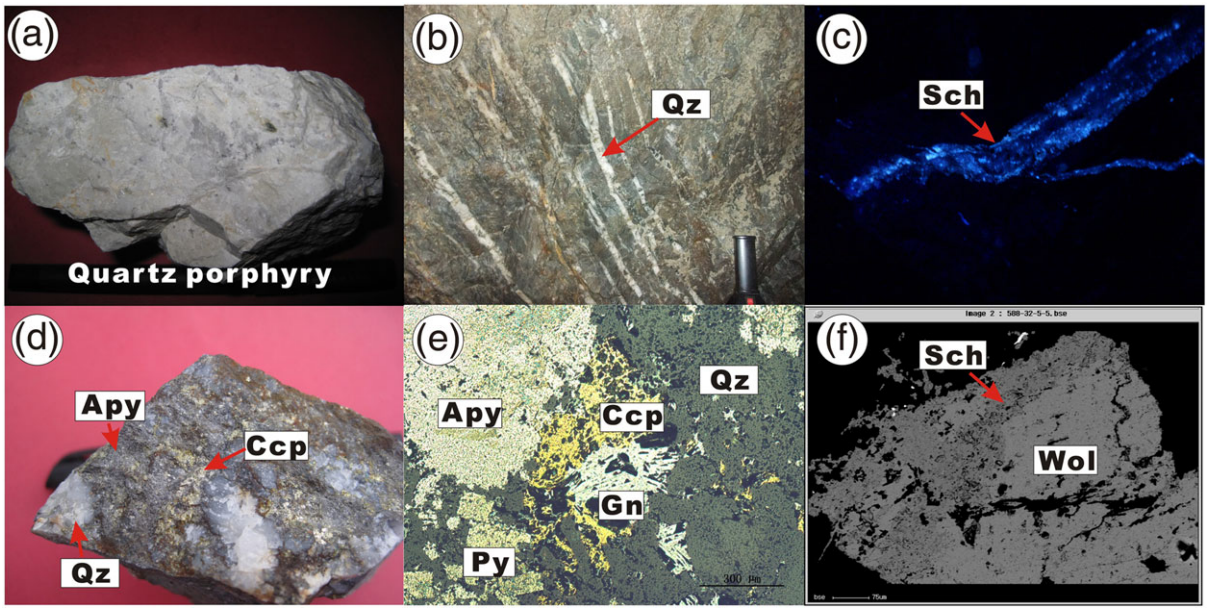

FIGURE 2 Photographs and photomicrographs of quartz porphyry, ores, and minerals assemblages of the DMJS deposit. (a) Quartz porphyry; (b) W-bearing quartz (Qz) veins; (c) W-bearing quartz veins under fluorescent light; (d) arsenopyrite (Apy) and chalcopyrite (Ccp) under the hand specimen. (e) arsenopyrite intergrowths with chalcopyrite, pyrite (Py), and galena (Gn), and its formation earlier than other sulphides (reflected light); (f) scheelite (Sch) intergrowths with wolframite (Wol) (back scattered electron images) [Colour figure can be viewed at wileyonlinelibrary.com]

type—the tungsten mineralization is dominated but with a spot of copper–arsenic, molybdenum, bismuth, lead, zinc mineralization which do not constitute industrial concentration. Alterations are complex and mainly silication, associated with sericitization, pyritization, and pyrrhotitization, always appearing on the middle-upper part of mining, such as middle of levels 803, 760, and 726; (c) compound type—the tungsten mineralization and copper–arsenic mineralization are superimposed, associated with lead–zinc mineralization, and they all have attained industrial concentration. Alterations are complex and pyritization, sericitization are comparatively developed except for silicatization, always appearing on the lower-middle part of mining, such as middle of levels 588 and 541. Single type is the most important mineralization type in the DMJS deposit.

3 | SAMPLING AND ANALYTICAL METHODS

3.1 | Sampling

Samples collected from the W-bearing and Cu–As-bearing quartz veins of the DMJS deposit were first crushed. Pyrite, galena, chalcopyrite, arsenopyrite, sphalerite, pyrrhotite, molybdenite, bismuthinite, and quartz were hand-picked under a binocular microscope. The purity of single mineral separate is over 99%. All mineral separates were cleaned in an ultrasonic bath before being grinded in an agate mortar. Pyrite, galena, chalcopyrite, arsenopyrite, sphalerite, pyrrhotite, molybdenite, and bismuthinite separates were analysed for S isotope compositions; pyrite, chalcopyrite, arsenopyrite, and pyrrhotite separates for He–Ar isotopic compositions; and quartz separates for H–O isotope compositions. He–Ar and S isotope analyses were performed at the State Key Laboratory of Ore Deposit Geochemistry, Institute of Geochemistry, China Academy of Sciences, Guiyang, China. H–O and Pb isotope compositions were measured at the Analytical Laboratory of Beijing Research Institute of Uranium Geology.

3.2 | Analytical methods

3.2.1 | S isotope

Sulphur isotopic analyses of sulphide minerals were carried out at the Institute of Geochemistry, Chinese Academy of Sciences, by using Continuous Flow Mass Spectrometer. GBW 04415 and GBW 04414 Ag_2S were used as the external standards, and the relative errors (2σ) were better than 0.2‰ from the replication of standard materials. Sulphur isotopic compositions are reported relative to Canyon Diablo Troilite (CDT).

3.2.2 | Pb isotope

Nine sulphide samples with similar occurrences as that of the S isotope samples were used to determine the Pb isotope compositions. The samples were dissolved in a mixed solution of hydrofluoric acid and perchloric acid, followed by basic anion exchange resin to purify Pb. Next, the samples were analysed using an ISOP-ROBE-T Thermal Ionization Mass Spectrometer instrument (Zhou, Huang, Zhou, Li, & Jin, 2013). The data of Pb isotopic compositions were provided in the form of (value ± 2σ). The precisions for $^{204}Pb/^{206}Pb$ and $^{208}Pb/^{206}Pb$ are better than 0.005%.

3.2.3 | H–O isotopes

Oxygen was liberated from quartz by reaction with BrF_5 (Clayton & Mayeda, 1963) and converted to CO_2 on a platinum-coated carbon rod. The oxygen isotopic determinations were made on a Finnigan MAT 253 mass spectrometer. Reproducibility for isotopically homogeneous pure quartz is about ±0.2‰ (1σ). Hydrogen isotope ratios on bulk fluid inclusions in quartz were measured by mechanical crushing of about 1 g of quartz grains, 1 to 5 mm in size, according to the method described by Simon (2001). Samples were first degassed of labile volatiles and secondary fluid inclusions by heating under vacuum to 120°C for 3 hr. The released water was trapped, reduced to H_2 by zinc, and then analysed with a Finnigan MAT 253 mass spectrometer at the Stable Isotope Laboratory of Beijing Research Institute of Uranium Geology. Analyses of standard water samples suggest a precision for δD of ±2‰ (1σ). With the continuous improvement of stable isotope testing technology and accuracy in recent years, the method has been applied to reveal the source and evolution of ore-forming fluid, and the process of mineralization.

3.2.4 | He–Ar isotopes

An all metal extraction line and mass spectrometer (GV5400) at the Institute of Geochemistry, Chinese Academy of Sciences, Guiyang, was used. The analytical methods used here were similar to those described in Burnard, Stuart, Ayliffe, and Turner (1993); Stuart, Burnard, Taylor, and Turner (1995), and Stuart, Turner, Duckworth, and Fallick (1994). Approximately 500–1,000 mg of separated coarse grained (generally 0.5–1.5 mm, but the coarser the better) pyrite, chalcopyrite, arsenopyrite, and pyrrhotite grains were cleaned ultrasonically in alcohol, dried, then loaded in online in vacuo crusher buckets. The samples were baked at 150°C onlined with the ultra-high vacuum system for >24 hr prior to analysis in order to remove adhered atmospheric gases. Gases were released from the grains into the all metal extraction system by sequential crushing in modified Nupro-type valves. The released gases were exposed to a titanium sponge furnace at 800°C for 20 min to remove the bulk of active gases (e.g., H_2O and CO_2) and then exposed to two SAES Zr–Al getters (one at room temperature, the other at 450°C) for 10 min to further purify. He was separated from Ar using an activated charcoal cold finger at liquid N_2 temperature (−196°C) for 40–60 min to trap Ar. He and then Ar isotopes and abundances were analysed on the GV 5400. Gas abundances were measured by peak height comparison with known amounts of standard air from an air bottle. He and Ar abundances and isotopic ratios were calibrated against pipettes of 0.1 cm^3 STP air (5.2×10^{-7} cm^3 STP ^4He and 9.3×10^{-4} cm^3 STP ^{40}Ar). Procedural blanks were $<2 \times 10^{-10}$ cm^3 STP ^4He and $(2–4) \times 10^{-10}$ cm^3 STP ^{40}Ar, and constituted <1% of analyses. The blank is too low to affect calibration of the abundance measurement (Hu et al., 2012).

4 | RESULTS

4.1 | S isotopic composition

The sulphur isotopic results are given in Table 1 and Figure 3. In the DMJS deposit, chalcopyrite, arsenopyrite, pyrite, and galena are the dominant sulphide ore minerals, so the $\delta^{34}S$ values of these sulphides can be considered approximately equal to that of hydrothermal fluids. The $\delta^{34}S$ values have a smaller range in the histogram (Figure 3). The sulphur isotope compositions are characterized by $\delta^{34}S$ deficiency, with values of $\delta^{34}S$ between −6.2‰ and 0‰ (Table 1). No obvious variations in the $\delta^{34}S$ values exist in the deposit. The relatively homogeneous sulphur isotopic compositions probably indicate a consistent sulphur source for the W–Cu–As polymetallic deposit.

4.2 | Pb isotopic composition

The Pb isotopic compositions are presented in Table 2 and Figure 4. The $^{206}Pb/^{204}Pb$, $^{207}Pb/^{204}Pb$, and $^{208}Pb/^{204}Pb$ ratios of the sulphides vary from 17.203 to 18.245, 15.402 to 15.726, and 37.541 to 38.422, respectively. The $^{206}Pb/^{204}Pb$, $^{207}Pb/^{204}Pb$, and

TABLE 1 Sulphur isotope compositions of the Damajianshan W–Cu–As polymetallic deposit

Mineral	$\delta^{34}S_{V\text{-}CDT}$‰	Mineral	$\delta^{34}S_{V\text{-}CDT}$‰	Mineral	$\delta^{34}S_{V\text{-}CDT}$‰	Mineral	$\delta^{34}S_{V\text{-}CDT}$‰	Mineral	$\delta^{34}S_{V\text{-}CDT}$‰
Pyr	−2.04	Py	−0.30	Py	−4.77	Ccp	−1.56	Bm	−3.93
Pyr	−3.47	Apy	−0.25	Py	−1.05	Ccp	−1.94	Mol	−5.05
Pyr	−3.36	Apy	−0.51	Ccp	−0.15	Ccp	−1.30	Mol	−1.74
Pyr	−2.50	Apy	−0.27	Ccp	−3.48	Ccp	−2.11	Mol	−4.66
Pyr	−2.16	Apy	−0.09	Ccp	−1.48	Ccp	−1.28	Mol	−4.36
Apy	−0.49	Apy	−0.46	Ccp	−0.93	Ccp	−1.62	Mol	−3.99
Apy	−0.18	Apy	−0.65	Ccp	−1.91	Ccp	−1.38	Mol	−4.42
Apy	−0.39	Apy	−0.97	Ccp	−0.95	Ccp	−1.56	Mol	−5.26
Apy	−0.47	Gn	−3.07	Ccp	−1.04	Ccp	−1.89	Mol	−3.50
Apy	−0.43	Gn	−3.03	Ccp	−1.40	Ccp	−3.19	Mol	−6.00
Apy	−0.37	Gn	−3.82	Ccp	−1.26	Ccp	−0.80	Mol	−6.17
Apy	−0.19	Gn	−2.92	Ccp	−1.01	Ccp	−1.05	Mol	−3.37
Apy	0.02	Py	−1.08	Ccp	−1.47	Ccp	−1.32	Mol	−3.38
Apy	−0.20	Py	−0.06	Ccp	−1.91	Ccp	−2.15	Mol	−4.20
Apy	−0.28	Py	−0.44	Ccp	−1.88	Ccp	−1.86	Mol	−5.29
Apy	−0.07	Py	−0.79	Ccp	−2.02	Ccp	−1.96	Mol	−4.27
Apy	−0.36	Py	−0.35	Ccp	−1.50	Ccp	−2.65	Sp	−1.52
Apy	−0.02	Py	−0.20	Ccp	−1.27	Ccp	−0.32	Sp	−2.03
Apy	−0.26	Py	−2.52	Ccp	−1.22	Ccp	−1.09	Sp	−3.52
Apy	−0.22	Py	−3.84	Ccp	−2.86	Ccp	−1.15	Sp	−2.13
Apy	−0.38	Py	−4.93	Ccp	−2.11	Ccp	−2.09		
Apy	0	Py	−0.64	Ccp	−2.40	Ccp	−1.85		

Note. Apy = arsenopyrite; Bm = bismuthinite; Ccp = chalcopyrite; Gn = galena; Mol = molybdenite; Py = pyrite; Pyr = pyrrhotite; Sp = sphalerite.

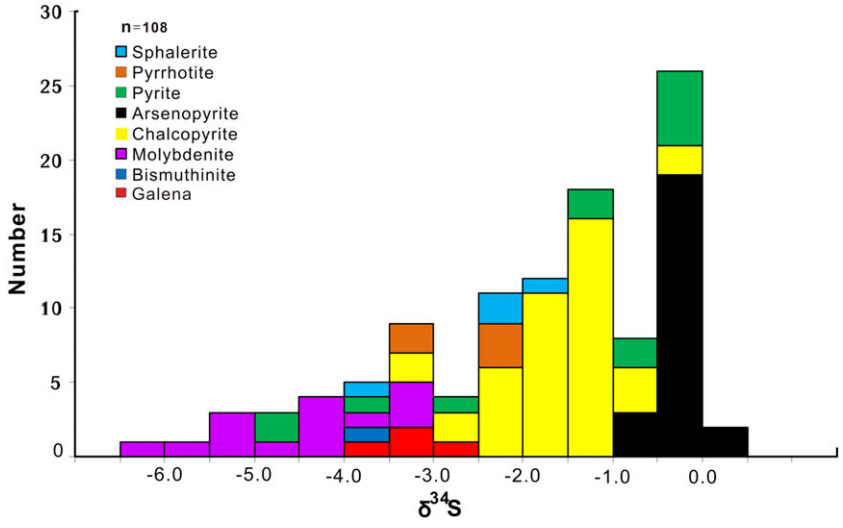

FIGURE 3 Histogram of the sulphur isotope compositions of sulphides from the Damajianshan deposit [Colour figure can be viewed at wileyonlinelibrary.com]

TABLE 2 Pb isotope compositions of sulphides and quartz porphyry from the Damajianshan deposit [Colour table can be viewed at wileyonlinelibrary.com]

Sample	Mineral	$^{208}Pb/^{204}Pb$	2σ	$^{207}Pb/^{204}Pb$	2σ	$^{206}Pb/^{204}Pb$	2σ
Sulphides							
462–6	Ccp	37.661	0.005	15.441	0.002	17.214	0.002
512–8	Ccp	37.679	0.008	15.446	0.003	17.217	0.003
462–7	Apy	37.541	0.005	15.402	0.002	17.203	0.002
512–10	Apy	37.885	0.006	15.459	0.003	17.402	0.002
512–11	Py	38.386	0.004	15.726	0.002	18.171	0.002
726–12	Py	38.343	0.005	15.707	0.002	18.154	0.002
512–16	Mol	38.422	0.004	15.684	0.002	18.245	0.002
462-kb	Sp	38.376	0.005	15.714	0.002	18.164	0.002
Quartz porphyry							
512–12		38.814	0.006	15.708	0.002	18.287	0.002
512–14		38.700	0.003	15.692	0.001	18.232	0.002
588–3		38.701	0.005	15.689	0.002	18.231	0.003
726–3		38.448	0.004	15.679	0.002	17.962	0.002
760–1		38.668	0.004	15.696	0.001	18.228	0.002

Note. The age of quartz porphyry is 228.7 ± 3.8 Ma (MSWD = 0.66; will be published elsewhere). λU238 = 0.155125 × 10−9 year-1, λU235 = 0.98485 × 10−9 year-1, λTh232 = 0.049475 × 10−9 year-1 (Steiger & Jäger, 1977).

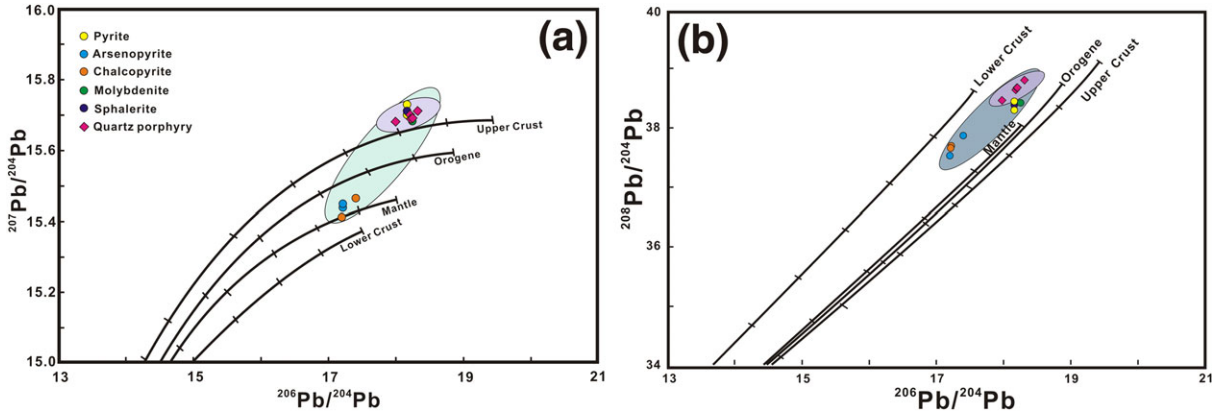

FIGURE 4 (a) $^{207}Pb/^{204}Pb$ versus $^{206}Pb/^{204}Pb$ diagram and (b) $^{208}Pb/^{204}Pb$ versus $^{206}Pb/^{204}Pb$ diagram of sulphides and quartz porphyry from the Damajianshan tungsten polymetallic deposit. Lead isotope curves for the upper crust, lower crust, orogene, and mantle are from Zartman & Doe, 1981 [Colour figure can be viewed at wileyonlinelibrary.com]

$^{208}Pb/^{204}Pb$ ratios of quartz porphyry which related to mineralization vary from 17.962 to 18.287, 15.679 to 15.708, and 38.448 to 38.814, respectively. The Pb isotope ratios of the quartz porphyry exhibit narrow ranges, but the Pb isotopic data of the sulphide samples were plotted over a wide range covering the mantle, orogene, and upper crustal reservoirs. This indicates that the lead source is multiple. The data present a quite good linear correlation, which probably indicates the mixing of variable proportions of mantle, orogenic belt, and upper crust lead, and the lead was derived from upper crust mainly mixed with a little from the mantle.

4.3 | H–O isotopic compositions

The $\delta^{18}O_{fluid}$ values were calculated from the $\delta^{18}O$ values of quartz, based on the formation temperatures of quartz (220–330°C) determined on fluid inclusions, using an equation for quartz–water isotopic equilibrium (Clayton, O'Neil, & Mayeda, 1972). The calculated oxygen isotope composition of the fluid varies between −5.5‰ and +9.2‰ (Table 3). The analyses of hydrogen isotopic composition, measured directly on inclusion fluid, gave a relatively narrow spread between −81.7‰ and −50.2‰. In a plot of δD versus $\delta^{18}O_{fluid}$ (Figure 5), quartz samples are plotted in the area between the meteoric water line and the primary magmatic water area but near the magmatic water area. This may reflect the increasing influence of meteoric water during the evolution of the ore-forming fluid (Figure 6).

4.4 | He–Ar isotopic compositions

He and Ar isotopic compositions and concentrations in samples were given in Table 4 and Figures 7 and 8. All samples show $^{3}He/^{4}He$ ratios are between 0.020 and 0.049 Ra (average 0.034, Ra is $^{3}He/^{4}He$ ratio in the atmosphere: 1.399×10^{-6}, Figures 7 and 8). The $^{40}Ar/^{36}Ar$ ratios in all samples range from 562.47–4159.14 (average 2022.34), which is greater than the air value of 295.5. One disadvantage of the crushing

TABLE 3 Oxygen and hydrogen isotope compositions of quartz from the Damajianshan tungsten polymetallic deposit

Sample	T (°C)	$\delta^{18}O_{Mineral}$ (‰)	$\delta^{18}O_{Fluid}$ (‰)	δD_{Fluid} (‰)	Sample	T (°C)	$\delta^{18}O_{Mineral}$ (‰)	$\delta^{18}O_{Fluid}$ (‰)	δD_{Fluid} (‰)
462–1	330	13.3	6.9	−67.9	588–6	300	13.3	5.9	−81.0
462–4	330	11.1	4.7	−75.9	588–32	300	12.8	5.4	−73.0
462–8	330	11.9	5.5	−75.5	628–4	280	12.3	4.2	−73.1
512–4	320	12.6	5.9	−68.0	628–7	280	12.0	3.9	−65.7
512–5	320	11.8	5.1	−71.1	628–10	280	11.6	3.5	−67.7
512–8	320	14.2	7.5	−79.0	726–5	240	9.4	−0.5	−58.3
512–10	320	13.6	6.9	−65.6	726–12	240	9.4	−0.5	−81.7
512–17	320	12.4	5.7	−78.4	760–7	220	10.8	−0.2	−52.5
512–19	320	13.4	6.7	−64.7	976–5	220	10.3	−0.7	−50.2
541–1	300	12.8	6.1	−71.3	1026–3	220	8.6	−2.4	−61.2
541–2	300	10.2	3.5	−64.2	1026–4	220	9.0	−2.0	−60.8
588–1	300	12.4	5.0	−81.0	1026–5	220	5.5	−5.5	−69.3
588–2	300	13.6	5.9	−76.2					

Note. Temperatures are based on fluid inclusion microthermometry; $\delta^{18}O$ fluid was calculated according to the equation: $1{,}000\ln\alpha_{quartz\text{-}water} = 3.38 \times 10^6/T^2 - 2.9$ (Clayton et al., 1972).

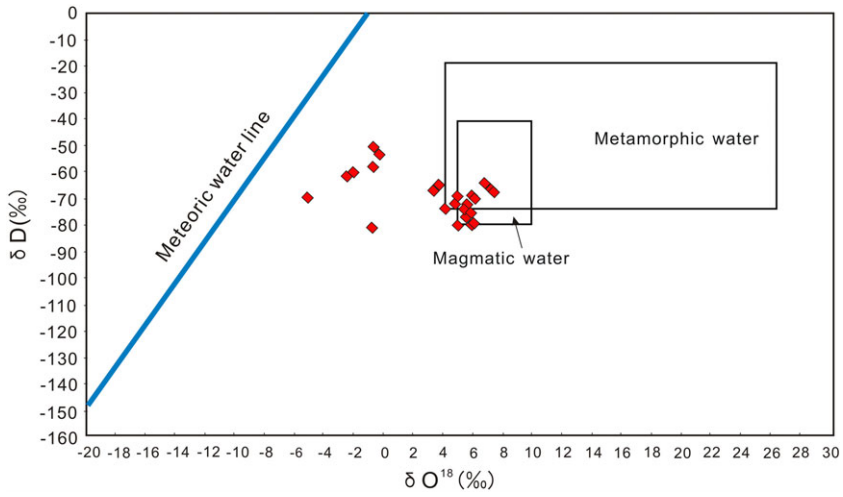

FIGURE 5 Hydrogen versus oxygen isotope diagram showing the compositions of hydrothermal fluids for W-bearing quartz veins from the Damajianshan deposit. Meteoric water line and primary magmatic water box are taken from Craig (1961) [Colour figure can be viewed at wileyonlinelibrary.com]

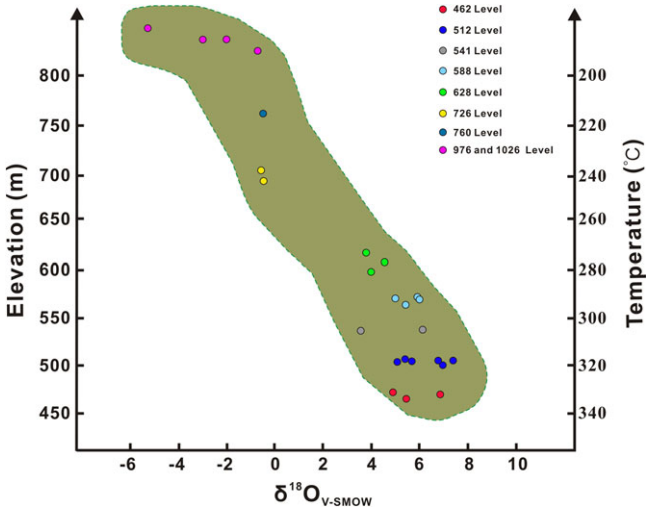

FIGURE 6 The relations between temperature, $\delta^{18}O_{fluid}$ values, and level at the Damajianshan deposit [Colour figure can be viewed at wileyonlinelibrary.com]

analytical technique is the difficulty to separate different generations of fluid inclusions in the sample, and the results represent some averaging of all fluid inclusions crushed (Burnard & Polya, 2004). Cosmogenic He is produced in the uppermost 1.5 m of the earth's surface (Kurz, 1986). The research samples used in this study were collected from underground tunnels at different levels, so cosmogenic He as a source of high $^3He/^4He$ can be ruled out. Because of the absence of any Li-bearing phases in the study area, nucleogenic ^3He can also be ignored (Simmons, Sawkins, & Schlutter, 1987; Stuart et al., 1995). The isotope fractionation caused by diffusing of He–Ar in the fluid inclusion and epigenetic superimposed He and Ar can also be ignored (Hu, Burnard, Turner, & Bi, 1998).

5 | DISCUSSION AND CONCLUSIONS

5.1 | Source of the ore-forming fluids

Although the $\delta^{34}S$ values of individual sulphides cannot indicate their source, the $\delta^{34}S$ value of total S (i.e., ΣS) in the fluids may be diagnostic (Ohomoto, 1972). In hydrothermal systems, where H_2S is the dominant sulphur species in the fluids or the fluid redox state is below the SO_2/H_2S boundary, a relation exists as $\delta^{34}S$ (sulphide) = $\delta^{34}S$ (fluid; Kelly & Rye, 1979). This means that the $\delta^{34}S$ values of sulphide minerals approximate those of the hydrothermal fluids. Therefore, these

TABLE 4 He and Ar isotopic compositions of inclusion-trapped fluid in pyrite, chalcopyrite, arsenopyrite, and pyrrhotite from the Damajianshan tungsten polymetallic deposit

Sample	Mineral	$^{3}He \times 10^{-13}$ (cm^3 STP/g)	$^{4}He \times 10^{-6}$ (cm^3 STP/g)	$^{36}Ar \times 10^{-10}$ (cm^3 STP/g)	$^{40}Ar \times 10^{-7}$ (cm^3 STP/g)	$^{3}He/^{4}He$ (Ra)	$^{40}Ar/^{36}Ar$	$^{3}He/^{36}Ar$ (10^{-3})	$^{40}Ar^{*}/^{4}He$
512–20	Py	3.1515	4.5992	4.7792	7.3120	0.049	1529.95	0.659	0.128
726–8	Py	1.5480	3.6047	6.1432	6.4462	0.031	1049.33	0.252	0.128
976–2	Py	9.3940	22.8750	9.5473	8.7427	0.030	915.73	0.984	0.026
462–6	Ccp	1.7432	2.7471	0.9567	3.7164	0.046	3884.84	1.822	0.125
512–4	Ccp	1.5940	5.7949	1.4675	6.1036	0.020	4159.14	1.086	0.098
512–7	Ccp	3.3369	6.8779	2.4865	5.3626	0.035	2156.67	1.342	0.067
512–8	Ccp	12.2580	37.0380	12.6780	42.3900	0.024	3343.54	0.967	0.104
512–10	Apy	0.4461	0.9067	5.0106	2.8183	0.035	562.47	0.089	0.148
628–5	Apy	1.3991	2.2936	2.4064	4.6929	0.044	1950.13	0.581	0.174
462-kb	Pyr	0.0861	0.2134	0.6328	0.4250	0.029	671.59	0.136	0.111

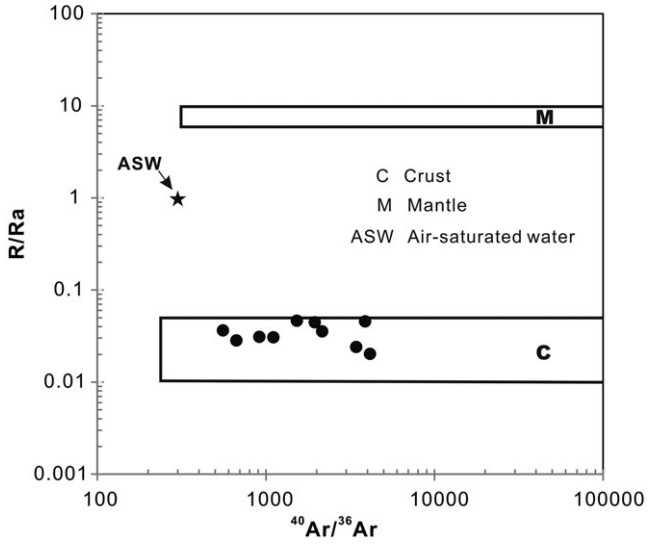

FIGURE 7 Plot of $^{3}He/^{4}He$ (R/Ra) versus $^{40}Ar/^{36}Ar$ ratios of fluids inclusions obtained from sulphides of the Damajianshan deposit

values can be used directly as representative of the sulphur source. In the DMJS deposit, pyrite, galena, chalcopyrite, arsenopyrite, sphalerite, pyrrhotite, molybdenite, and bismuthinite are the dominant ore minerals, so the $\delta^{34}S$ values of sulphides can be considered approximately

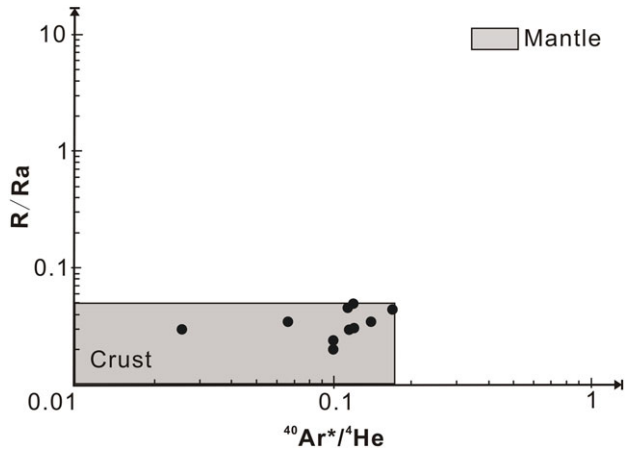

FIGURE 8 Plot of $^{3}He/^{4}He$ (R/Ra) versus $^{40}Ar^{*}/^{4}He$ ratios of fluids inclusions obtained from sulphides of the Damajianshan deposit [Colour figure can be viewed at wileyonlinelibrary.com]

equal to that of the hydrothermal fluids. The $\delta^{34}S$ values of the sulphides are slightly negative (Table 1 and Figure 3). The bulk of the $\delta^{34}S$ values are restricted to the interval of −6.2‰ to 0‰ (average − 1.9‰). Traditionally, a $\delta^{34}S$ value of about 0‰ is taken as indicative of a magmatic fluid, so the $\delta^{34}S$ values of the DMJS deposit indicate that the sulphur in the ores was derived from a magmatic source, and the alumina saturation index (ACNK) of quartz porphyry related to mineralization is 1.1–2.5 which reflect that the magma derived from the partial melting of the continental crust (Table 5).

The $\delta^{18}O$ values of W-bearing quartz veins range from +5.5‰ to +16.6‰. Their δD values vary from −81.7‰ to −50.2‰. The $\delta^{18}O_{fluid}$ values of the fluid are calculated from the $\delta^{18}O$ values of hydrothermal quartz based on the fluid inclusion temperatures of 190–330°C and the oxygen fractionation equation of Clayton et al. (1972). The calculated values are between −5.5‰ and +7.5‰, a range between the magmatic domain and the meteoric water line (Figure 5). The magnitude of the dispersion in $\delta^{18}O_{fluid}$ values may be due to mixing of magmatic water and Mesozoic meteoric water. Hydrogen versus oxygen isotope diagram is shown in Figure 5. The values of $\delta^{18}O_{fluid}$ show a trend of decreasing from deep to shallow as the metallogenic temperature decreases and showing that the proportion of meteoric water increased towards the shallow (Figure 6). The ore-forming temperature decreases gradually upward. The $\delta^{18}O_{fluid}$ values of ore-forming fluids increase and $\delta^{18}D$ values lower from shallow to deep (Zhang, 1985). Figure 5 shows that in the ore-forming fluids, the hydrogen isotope composition presents a little change, but the oxygen isotope decreases significantly in the DMJS deposit. These may be caused by the mixing of the local meteoric water.

The isotopic composition of the noble gases can be used as an ideal tracer for the crust and mantle contributions to the ore-forming processes (Stuart et al., 1995; Turner et al., 1993). Noble gases in inclusion-trapped fluids have three potential sources, notably air-saturated water, mantle-derived fluids, and crust-derived fluids (Burnard, Hu, Turner, & Bi, 1999; Stuart et al., 1995; Turner et al., 1993). The amount of helium in the atmosphere is too low to exert a significant influence on the He abundances and isotopic compositions of most crustal fluids (Marty, Jambon, & Sano, 1989; Stuart et al., 1994). Helium in the ore-forming fluids of the deposit

TABLE 5 Part data of the major (wt%) and trace elements ($\times 10^{-6}$) analyses of the Damajianshan quartz porphyry [Colour table can be viewed at wileyonlinelibrary.com]

Sample	Lithology	N	K_2O	Na_2O	CaO	Al_2O_3	SiO_2	Y	Yb	Rb	Nb	Ta	A/CNK
512	Porphyry	3	4.57	1.91	0.8	12.57	74.28	18.67	2.27	352.33	17.07	2.20	1.31
588	Porphyry	2	8.53	1.08	0.28	12.19	74.88	22.70	2.36	342.50	15.80	2.01	1.05
726	Porphyry	3	8.82	1.03	0.34	12.46	74.92	16.43	1.69	242.83	15.07	1.75	1.04
760	Porphyry	1	6.25	2.35	0.50	12.98	74.57	15.50	1.48	325.00	19.70	1.95	1.12
803	Porphyry	1	6.88	1.32	0.22	11.79	76.55	12.60	1.23	377.00	14.00	1.56	1.17
976	Porphyry	1	5.82	0.15	0.02	12.97	74.02	21.30	2.29	470.00	18.50	2.32	1.96
1026	Porphyry	1	7.58	1.50	0.09	13.14	75.65	13.30	1.50	368.00	16.50	1.77	1.21

Note. The data are the average value. N = number of the samples.

could have only two possible sources: mantle and crust. In this study, the results show a $^3He/^4He$ ratio of 0.020 to 0.049 R/Ra, which fall within the range of continental crust (0.01–0.05 R/Ra) but are significantly lower than those of air-saturated water (1 R/Ra) and the normal mantle (6–9 R/Ra). The R/Ra values suggest that crustal fluids played an important rule during the mineralization of the DMJS deposit (Figures 7 and 8). The measured $^{40}Ar/^{36}Ar$ values of fluid inclusions obtained from sulphides of the DMJS deposit range from 562.47 to 4,159.14. Compared with low atmospheric values (295.5), the higher $^{40}Ar/^{36}Ar$ values indicate a significantly higher concentration of $^{40}Ar^*$ (radiogenic ^{40}Ar) of mantle or crustal sources. Most $^{40}Ar^*/^4He$ values are between 0.026 and 0.174, the average $^{40}Ar^*/^4He$ value of 10 samples is 0.111 (Table 5) and are all lower than the crustal $^{40}Ar^*/^4He$ production ratio of 0.2. The $^{40}Ar^*/^4He$ versus R/Ra plot (Figure 8) shows the data points distributed in the area of crustal fluid. The variations of $^3He/^4He$ ratios change slightly. These features indicate that the ore-forming fluid may be mainly derived from crustal fluid mixed with some amounts of air-saturated water, but there was no considerable involvement of mantle-derived fluid.

5.2 | Source of the ore metals

Pb isotopes are useful in assessing the source of ore metals, providing important information about the nature of Pb reservoir(s) and defining a geotectonic environment for the ore deposits (Ballentine, Burgess, & Marty, 2002; Wang et al., 2015). The Pb isotopic composition of sulphides from the DMJS deposit span a wide range, suggesting a multiple source. On the $^{207}Pb/^{204}Pb$–$^{206}Pb/^{204}Pb$ and $^{208}Pb/^{204}Pb$–$^{206}Pb/^{204}Pb$ diagrams (Figure 4), all of the sulphides are distributed in the domain between the upper crust and the mantle curve and present a quite good linear correlation, which probably indicates mixing of variable proportions of mantle, orogenic belt, and upper crust lead. The

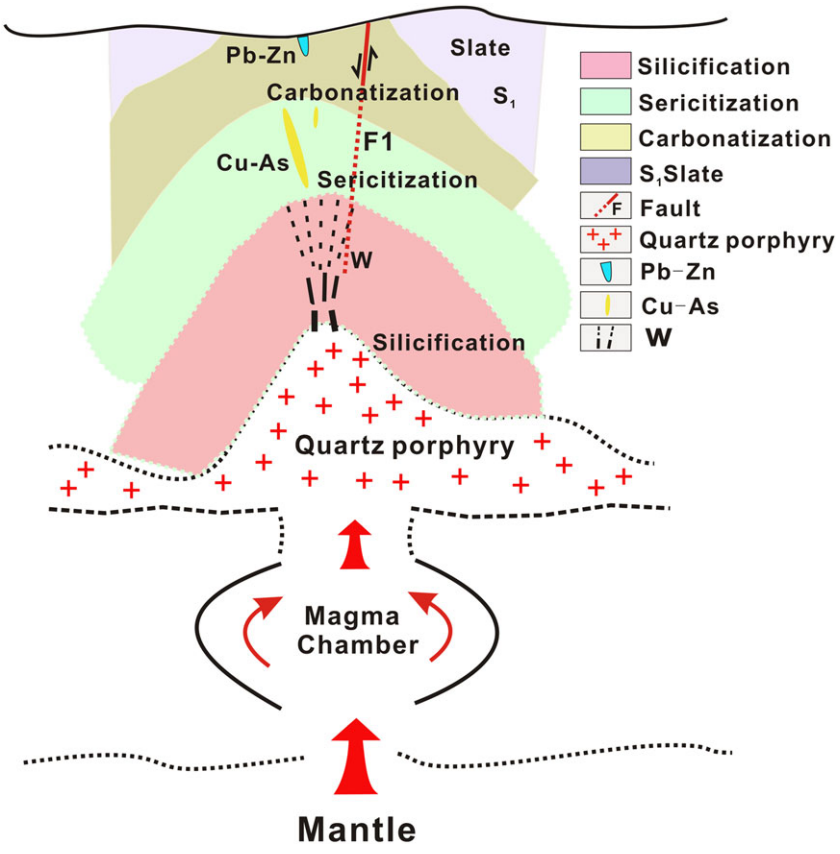

FIGURE 9 Sketch map of the metallogenic model of the Damajianshan tungsten polymetallic deposit [Colour figure can be viewed at wileyonlinelibrary.com]

ore-forming metals of the DMJS deposit might derive from the upper crust mainly mixed with a little from the mantle.

5.3 | Metallogenic model for the DMJS deposit

An integrated isotopic study of the DMJS deposit allow us to draw the following conclusions: (a) The $\delta^{34}S$ values of the hydrothermal sulphides indicate that the sulphur in the ore-forming fluids of the DMJS deposit was of a magmatic source and was primarily derived from the porphyry magma; (b) the δD and $\delta^{18}O_{fluid}$ values of ore-forming fluid indicate that the fluids responsible for the tungsten polymetallic mineralization were derived from a magmatic source and were mixed with a small amount of meteoric water after the main-ore stage; (c) He and Ar isotope compositions of the inclusions in sulphides from the DMJS deposit suggest that the ore-forming fluids in the main-ore stage are mainly crust-derived; (d) Combining all the H–O, He–Ar, and S isotope data from the DMJS deposit, we can confirm that the ore-forming fluids in the main-ore stage is primary from crust-derived porphyry magma and was mixed with a small amount of meteoric water after the main-ore stage; (e) the Pb isotopic compositions of sulphide minerals indicate that the ore-forming metals of the DMJS deposit were mainly derived from the deep crust and probably with a minor input of mantle materials.

Based on the above-mentioned discussions, the formation process of the DMJS deposit might be described as follows: The magmatic water rich in volatiles and ore-forming elements from the crystallization differentiation of granitic magma was mixed with a small amount of air-saturated water, which infiltrated through a large number of faults and fissures in the mining area. After that, the mixed fluids were heated and extracted metal elements from the wall rock in processes of deep circulation and then migrated upward. Once the physicochemical conditions changed, ore metals precipitated and mineralized at favourable tectonic positions. In the spatial distribution, from the quartz porphyry to outside and shallow, the ore bodies output W, Cu–As, and Pb–Zn, respectively (Figure 9). The regularity of ore bodies distribution have a well spatiality.

ACKNOWLEDGEMENTS

The authors acknowledge Guohao Jiang, Ning An, and Hanbin Liu for their help with isotopes analyses and explanation. We would like to express my gratitude to Doctor Haifeng Fan. This project was financially supported by the National Key R&D Program of China (2017YFC0602503), the strategic Priority Research Program (B) of Chinese Academy of Sciences (Grant No. XDB18030302), 973 Program (2014CB440904), Guizhou Scientific and Technological Innovation Team (2017-5657) and Fundamental Research Foundation of the Central Universities (300102278111 and 310827172003).

ORCID

Lei Zhang http://orcid.org/0000-0002-2673-1026
Guishan Zhang http://orcid.org/0000-0002-4813-1128
Rongxi Li http://orcid.org/0000-0003-1733-6048

REFERENCES

Ballentine, C. J., Burgess, R., & Marty, B. (2002). Tracing fluid origin, transport and interaction in the crust. *Review Mineral Geochemistry*, *47*(1), 539–614.

Burnard, P. G., & Polya, D. A. (2004). Importance of mantle derived fluids during granite associated hydrothermal circulation: He and Ar isotopes of ore minerals from Panasqueira. *Geochimica et Cosmochimica Acta*, *68*, 1607–1615.

Burnard, P.G., Stuart, F., Ayliffe, L., & Turner, G. (1993). Noble gas isotopic and elemental abundances in inclusion and vesicle trapped fluids: Method. *Abstract Supplement*, *Seventh meeting of the European Union of Geosciences*, *5*(Suppl. 1):368.

Burnard, P. G., Hu, R. Z., Turner, G., & Bi, X. W. (1999). Mantle, crustal and atmospheric noble gases in Ailaoshan gold deposits, Yunnan Province, China. *Geochimica et Cosmochimica Acta*, *63*, 1595–1604.

Clayton, R. N., & Mayeda, T. K. (1963). The use of bromine pentafluoride in the extraction of oxygen from oxides and silicates for isotopic analysis. *Geochimica et Cosmochimica Acta*, *27*, 43–52.

Clayton, R. N., O'Neil, J. R., & Mayeda, T. K. (1972). Oxygen isotope exchange between quartz and water. *Journal of Geophysical Research*, *77*(17), 3057–3067.

Craig, H. (1961). Isotope variations in meteric waters. *Science*, *133*, 1702–1703.

Deng, J., Hou, Z. Q., Mo, X. X., Yang, L. Q., Wang, Q. F., & Wang, C. M. (2010). Superimposed orogenesis and metallogenesis in Sanjiang Tethys. *Mineral Deposit*, *29*(01), 37–42. (in Chinese with English abstract)

Deng, J., Yang, L. Q., & Wang, C. M. (2011). Research advances of superimposed orogenesis and metallogenesis in the Sanjiang Tethys. *Acta Petrologica Sinica*, *27*(9), 2501–2509. (in Chinese with English abstract)

Deng, J., Wang, C. M., & Li, G. J. (2012). Style and process of the superimposed mineralization in the Sanjiang Tethys. *Acta Petrologica Sinica*, *28*(5), 1349–1361. (in Chinese with English abstract)

Deng, J., Wang, Q. F., Li, G. J., Li, C. S., & Wang, C. M. (2013). Tethys tectonic evolution and its bearing on the distribution of important mineral deposits in the Sanjiang region, SW China. *Gondwana Research*, *26*(214), 419–437.

Deng, J., Wang, C. M., Li, W. C., & Wang, Q. F. (2014). The situation and enlightenment of the research of the tectonic evolution and metallogenesis in the Sanjiang Tethys. *Earth Science Frontiers*, *21*(01), 52–64. (in Chinese with English abstract)

Hou, Z. Q., Wang, L. Q., Zaw, K., Mo, X. X., Wang, M. J., Li, D. M., & Pan, G. T. (2003). Post-collisional crustal extension setting and VHMS mineralization in the Jinshajiang orogenic belt, southwestern China. *Ore Geology Reviews*, *22*(3), 177–199.

Hou, Z. Q., Pan, X. F., Yang, Z. M., & Qu, X. M. (2007a). Porphyry Cu-(Mo-Au) deposits no related to oceanic-slab subduction examples from Chinese porphyry deposits in continental settings. *Geoscience*, *21*(02), 332–351. (in Chinese with English abstract)

Hou, Z. Q., Zaw, K., Pan, G. T., Mo, X. X., Xu, Q., Hu, Y. Z., & Li, X. Z. (2007b). Sanjiang Tethyan metallogenesis in SW China: Tectonic setting, metallogenic epochs and deposit types. *Ore Geology Reviews*, *31*(1), 48–87.

Hu, R. Z., Burnard, P. G., Turner, G., & Bi, X. W. (1998). Helium and argon systematics in fluid inclusions of Machangqing copper deposit in west Yunnan province, China. *Chemical Geology*, *146*, 55–63.

Hu, R. Z., Burnard, P. G., Bi, X. W., Zhou, M. F., Pen, J. T., Su, W. C., & Wu, K. X. (2004). Helium and argon isotope geochemistry of alkaline intrusion-associated gold and copper deposits along the Red River–Jinshajiang fault belt, SW China. *Chemical Geology*, *203*(3), 305–317.

Hu, R. Z., Bi, X. W., Jiang, G. H., Chen, H. W., Peng, J. T., Qi, Y. Q., … Wei, W. F. (2012). Mantle-derived noble gases in ore-forming fluids of the granite-related Yaogangxian tungsten deposit, Southeastern China. *Mineralium Deposita*, *47*(6), 623–632.

Kelly, W. C., & Rye, R. O. (1979). Geologic, fluid inclusion, and stable isotope studies of the tin-tungsten deposits of Panasqueira, Portugal. *Economic Geology*, *74*, 1721–1822.

Kurz, M. D. (1986). In situ production of cosmogenic helium and some applications to geochronology. *Geochimica et Cosmochimica Acta*, *50*, 2855–2862.

Li, Z. X., & Li, X. H. (2007). Formation of the 1300-km-wide intra-continental orogen and post-orogenic magmatic province in Mesozoic South China: A flat-slab subduction model. *Geology*, *35*, 179–182.

Li, H. Q., Liu, J. Q., & Wei, L. (1993). *Fluid inclusion chronology of hydrothermal deposit (in Chinese)*. (pp. 50–54). Beijing: Geological Publishing House. (in Chinese with English abstract)

Li, X. Z., Liu, W. J., & Wang, Y. Z. (1999). *Tethys tectonic evolution and mineralization in the Sanjiang area (pandect)*. (pp. 1–276). Beijing: Geological Publishing House. (in Chinese with English abstract)

Liu, Z. Q., Li, X. Z., & Ye, Q. T. (1993). *Division of tectono-magmatic zone and distribution of mineral in the Sanjiang Region*. (p. 246). Beijing: Geol. Pub. House. (in Chinese)

Marty, B., Jambon, A., & Sano, Y. (1989). Helium isotope and CO_2 in volcanic gases of Japan. *Chemical Geology*, *76*, 25–40.

Ohomoto, H. (1972). Systematics of sulfur and carbon isotopes in hydrothermal ore deposits. *Economic Geology*, *67*, 551–578.

Pan, G. T., Chen, Z. L., & Li, X. Z. (1997). *The tectonic evolution of eastern Tethys*. (pp. 28–101). Beijing: Geological Publishing House. (in Chinese with English abstract)

Pan, G. T., Wang, L. Q., Yin, F. G., Zhu, D. C., Geng, Q. R., & Liao, Z. L. (2004). Charming of landing of plate tectonics on the continent as viewed from the study of the archipelagic arc-basin system. *Geological Bulletin of China*, *23*(9–10), 933–939. (in Chinese with English abstract)

Qiu, H. N., Dai, M., & Pu, Z. P. (1994). Dating mineralization of Lushui Tin-tungsten Deposit, western Yunnan, using ^{40}Ar-^{39}Ar age spectrum technique. *Geochimica*, *23*(suppl), 93–102. (in Chinese with English abstract)

Simmons, S. F., Sawkins, F. J., & Schlutter, D. J. (1987). Mantle-derived helium in two Peruvian hydrothermal ore deposits. *Nature*, *329*, 429–432.

Simon, K. (2001). Does δD from fluid inclusion in quartz reflect the original hydrothermal fluids. *Chemical Geology*, *177*, 483–495.

Steiger, R. H., & Jäger, E. (1977). Subcommission on geochronology: Convention of the use of decay constants in geo- and cosmochronology. *Earth and Planetary Science Letters*, *36*, 359–362.

Stuart, F. M., Turner, G., Duckworth, R. C., & Fallick, A. E. (1994). Helium isotopes as tracers of trapped hydrothermal fluids in ocean-floor sulfides. *Geology*, *22*, 823–826.

Stuart, F. M., Burnard, P. G., Taylor, R. P., & Turner, G. (1995). Resolving mantle and crustal contributions to ancient hydrothermal fluids: He-Ar isotopes in fluid inclusions from Dae Hwa W-Mo mineralisation, South Korea. *Geochimica et Cosmochimica Acta*, *59*, 4663–4673.

Sun, X. M., Zhang, Y., Xiong, D. X., Sun, W. D., Zhai, W., & Wang, S. W. (2009). Crust and mantle contributions to gold-forming process at the Daping deposit, Ailaoshan gold belt, Yunnan, China. *Ore Geology Reviews*, *36*, 235–249.

Turner, G., Burnard, P. G., Ford, J. L., Gilmour, J. D., Lyon, I. C., & Stuart, F. M. (1993). Tracing fluid sources and interaction. *Philosophical Transactions of Royal Society*, *344*, 127–140.

Wang, C. M., Deng, J., Zhang, S. T., Xue, C. J., Yang, L. Q., Wang, Q. F., & Sun, X. (2010a). Sediment-hosted Pb-Zn deposits in southwest Sanjiang Tethys and Kangdian area on the western margin of Yangtze Craton. *Acta Geologica Sinica*, *84*(6), 1428–1438.

Wang, C. M., Deng, J., Zhang, S. T., & Yang, L. Q. (2010b). Metallogenic province and large scale mineralization of VMS deposits in China. *Resource Geology*, *60*, 404–413.

Wang, C. M., Deng, J., Carranza, E. J. M., & Santosh, M. (2014). Tin metallogenesis associated with granitoids in the southwestern Sanjiang Tethyan domain: Nature, deposit types, and tectonic setting. *Gondwana Research*, *26*(2), 576–593.

Wang, L. Q., Tang, J. X., Cheng, W. B., Chen, W., Zhang, Z., Lin, X., … Yang, C. (2015). Origin of the ore-forming fluids and metals of the Bangpu porphyry Mo–Cu deposit of Tibet, China: Constraints from He–Ar, H–O, S and Pb isotopes. *Journal of Asian Earth Sciences*, *103*, 276–287.

Xue, C. J., Zeng, R., Liu, S. W., Chen, Y. C., Yang, J. M., & Wang, D. H. (2007). Geologic, fluid inclusion and isotopic characteristics of the Jinding Zn–Pb deposit, western Yunnan, South China: A review. *Ore Geology Reviews*, *31*, 337–359.

Yin, G. F., Pan, G. T., Wang, F., Li, X. Z., & Wang, F. G. (2006). Tectonic facies along the Nujiang-Lancangjiang-Jinshajing orogenic belt in southwestern China. *Sedimentary Geology and Tethyan Geology*, *26*(4), 33–39. (in Chinese with English abstract)

Zartman, R. E., & Doe, B. R. (1981). Plumbotectonics—The model. *Tectonophysics*, *75*, 135–162.

Zaw, K., Peters, S. G., Cromie, P., Burrett, C., & Hou, Z. Q. (2007). Nature, diversity of deposit types and metallogenic relations of South China. *Ore Geology Reviews*, *31*, 3–47.

Zhang, L. G. (1985). Hydrogen, oxygen, sulfur and carbon isotope geochemistry of the Lianhuashan porphyry type tungsten deposit. *Mineral Deposits*, *4*(1), 54–63.

Zhang, L., Wen, H. J., Qin, C. J., Du, S. J., Zhu, C. W., … Zhang, J. R. (2015). The geological significance of Pb–Bi- and Pb–Sb-sulphosalts in the Damajianshan tungsten polymetallic deposit, Yunnan Province, China. *Ore Geology Reviews*, *71*, 203–214.

Zhou, J. X., Huang, Z. L., Zhou, M. F., Li, X. B., & Jin, Z. G. (2013). Constraints of C–O–S–Pb isotope compositions and Rb–Sr isotopic age on the origin of the Tianqiao carbonate-hosted Pb–Zn deposit, SW China. *Ore Geology Reviews*, *53*, 77–92.

How to cite this article: Zhang L, Zhang G, Wen H, et al. Genetic implications for the Damajianshan W-Cu-As polymetallic deposit in Lvchun, Southwest China: Constraints from H–O, He–Ar, S, and Pb isotopes. *Geological Journal*. 2018;1–11. https://doi.org/10.1002/gj.3187